

Demonstration of lithium niobate integration on a 200-mm silicon photonics wafer using transfer printing

MARGOT NIELS^{1,2*}, EWOUT VISSERS^{1,2}, TOM VANACKERE^{1,2}, ARNO MOERMAN^{2,3}, XIN GUO^{1,2}, PETER GEERINCK^{1,2}, EMADREZA SOLTANIAN^{1,2}, JING ZHANG^{1,2}, SOFIE JANSSEN², PETER VERHEYEN², NEHA SINGH², DIETER BODE², MARTIN DAVI², FILIPPO FERRARO², PHILIPPE ABSIL², SADHISHKUMAR BALAKRISHNAN², JORIS VAN CAMPENHOUT², SEBASTIAN HÄNSCH⁴, HANH MAI⁴, NISHANT SINGH^{2,3}, GÜNTHER ROELKENS^{1,2}, SARAH UVIN^{1,2}, MAXIMILIEN BILLET^{1,2}, AND BART KUYKEN^{1,2}

¹Department of Information Technology (INTEC) - Photonics Research Group, Ghent University–imec, Technologiepark Zwijnaarde 126, 9052 Ghent, Belgium.

²imec, Kapeldreef 75, 3001 Leuven, Belgium.

³Department of Information Technology (INTEC) - IDLab, Ghent University–imec, Technologiepark Zwijnaarde 126, 9052 Ghent, Belgium.

⁴Semiconductor Solutions ASMP/T, AMICRA, 93055 Regensburg, Germany.

*margot.niels@ugent.be

Compiled June 12, 2025

We present a scalable approach for the heterogeneous integration of lithium niobate onto silicon photonics platforms using wafer-scale micro-transfer printing. This approach enables the incorporation of efficient, high-speed modulators while maintaining compatibility with back-end processing. 7-mm-long electro-optic modulators, fabricated with this technology, achieve a half-wave voltage of 4 V and a bandwidth exceeding 70 GHz. Furthermore, as a proof of concept, we demonstrate the integration of more than 200 lithium niobate photonic structures directly on a 200-mm wafer and characterise their passive optical properties.

<http://dx.doi.org/10.1364/ao.XX.XXXXXX>

1. INTRODUCTION

The growing demand for faster optical components in data centres — with bandwidths expected to exceed 100 GHz — has driven the progress of the integration of photonic elements in transceivers [1–4]. In the field of photonic integration, silicon photonics has become a key platform as it allows for the integration of modulators, switches, photodetectors, and low-loss waveguides, using mature fabrication techniques. However, emerging standards challenge the limits of silicon-based modulators [5]. To address these limitations, various alternatives are explored including barium titanate [6], organic materials [7], plasmonics [8], III-V semiconductors [3], and graphene [9, 10]. Thin-film lithium niobate (TFLN) has gained prominence for its low optical loss and high-speed, efficient electro-optic response [11, 12]. However, high-volume production in CMOS fabs, required for the mass deployment of the next-generation data communication links, remains challenging due to the lithium-induced contamination [13]. Another approach is the heterogeneous integration of TFLN with established silicon photonics

technology. While scalable demonstrations using wafer bonding exist [14], they still require back-end etching of the TFLN waveguides. Sample-scale heterogeneous TFLN demonstrators using transfer printing [15, 16] have emerged as a versatile and promising solution for non-linear optics [17] and high-speed photonics [18–20] but are still in an early technological development stage, and the scalable integration on a 200-mm wafer has never been demonstrated.

This work introduces a back-end micro-transfer printing process for the integration of lithium niobate (LN) on a silicon photonics platform, enabling high-speed modulators with a low half-wave voltage (V_π) of 3.8 V for a length of 7 mm and a large bandwidth of more than 70 GHz. Also, the compatibility of this approach with scalability is illustrated with, as a proof of concept, over 200 photonic structures being integrated on a 200-mm wafer that are optically characterised.

2. A HIGH-SPEED HYBRID MODULATOR LEVERAGING AN LN ENHANCED SI-SiN PLATFORM

A. Concept of the heterogeneous Si-SiN/LN modulator

The modulator presented in this work is a hybrid SiN/LN (Si routing and SiN/LN modulating arms) unbalanced Mach-Zehnder modulator (MZM), as depicted in Fig. 1.a. The passive architecture of the modulator is based on a wafer-scale Si and SiN platform using the standard process design kit (PDK). It includes grating couplers, Si and SiN routing, multimode interferometer (MMI) splitters and adiabatic Si to SiN transitions. The LN material is integrated, as discussed in [19], using micro-transfer printing. This method allows for the integration of 300 nm thick LN slabs measuring 30 μm by 7 mm on the silicon photonics platform with the help of a benzocyclobutene (BCB) intermediate layer. Additionally, when using micro-transfer printing, the relative crystal orientation of the LN in each modulator arm is flipped so that we can achieve a push-pull configuration for the device. The light is coupled from the Si to

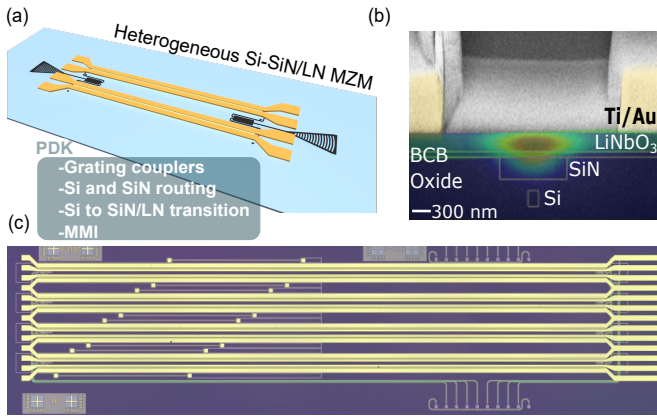


Fig. 1. Concept of a heterogeneous Si-SiN/LN modulator. (a) Schematic view of the heterogeneous Si-SiN/LN modulator. (b) Cross section of the Mach Zehnder modulator arm showing the hybrid SiN/LN optical mode. (c) Optical picture of a fabricated chip consisting of four modulators.

the hybrid SiN/LN optical mode using a bi-layer Si and SiN adiabatic transition. The LN allows for modulation through the electro-optic Pockels effect, while the SiN provides low-loss propagation. The hybrid arms are driven by an external electric field across two 1 μm thick gold electrodes with a gap of 5 μm , as illustrated in Fig.1.b. An example of a die incorporating four modulators, fabricated on a high resistivity silicon substrate is presented in Fig.1.c.

B. High-speed measurement of the lithium niobate modulator

First, the extinction ratio (ER) is measured by recording the optical transmission at wavelengths centred around 1310 nm. The light is coupled to and collected from the optical chip with optical fibres aligned to the in- and output polarisation-dependent grating couplers (GCs). The recording, displayed in Fig.2.a, shows an ER exceeding 25 dB. The transmission is normalised by removing the external insertion loss, described later and detailed in table 1.

The half wave voltage (V_{π}) is measured by conducting a quasi-DC electro-optic experiment on the 7 mm long devices for which an electrical signal generator generates a 100 kHz signal driving the device. The laser light is again coupled into the MZM through a fibre-GC and its wavelength is tuned to 1309.38 nm to bias the MZM in its quadrature point. The optical power transmitted through the MZM is converted to an electrical signal by a photodiode (PD). Both the electrical signal driving the device and the one registered by the PD are recorded on an oscilloscope, allowing to obtain the correlation between the transmitted power as a function of the input voltage, as presented in Fig.2.b. The resulting V_{π} is 4 V, which corresponds to a half-wave voltage length product ($V_{\pi}L$) of 2.6 V.cm.

The high-speed characteristic is measured in an electrical-optical-electrical (EOE) experiment, where the same setup is used as for the V_{π} characterisation, but with a faster PD and with a vectorial network analyser (VNA) to generate and record the electrical signals. The recorded data is reported in Fig.2.c and shows a 3 dB EOE response of the 7 mm device exceeding 70 GHz that is limited by the bandwidth of the measurement devices.

Component	Loss [dB]
External routing	1.0 ± 0.4
MMI splitters	0.2 ± 0.2
Si routing inside MZM	2.7 ± 0.4
Transitions (Si to SiN/LN)	0.3 ± 0.1
EO section (SiN/LN)	0.5 ± 0.3

Table 1. Loss characteristics of the Si-SiN/LN modulator at 1310 nm

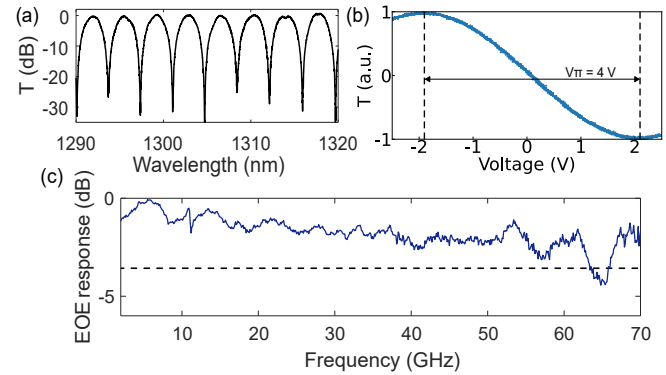


Fig. 2. Characterisation of a typical heterogeneous Si-SiN/LN MZM. (a) Extinction ratio. (b) Half wave voltage (c) EOE bandwidth.

3. WAFER-SCALE INTEGRATION ON A 200-MM PLATFORM

A. Demonstration of lithium niobate integration

The approach presented in this work is compatible with the integration of LN on wafers of 200 mm and 300 mm diameter, using a commercial transfer printing tool. The pre-processed LN devices do not use LN tethering, seen as a source of contamination in fabs, and do not require any modification of the 200-mm silicon photonic wafer preparation for the heterogeneous integration. As a proof of concept, we demonstrate the integration of 217 coupons of LN on a 200-mm commercial silicon wafer with an integration yield of 99% on a mixture of cut-back structures and modulator structures. A quarter of a full 200-mm wafer is printed, demonstrating the stability of the process for positions at the extreme locations in both the horizontal and vertical directions relative to the centre. One device in the demonstration has not been successfully bonded, because of a local defect at the printing location that was present before the printing. This result demonstrates the first integration of LN on a commercial 200 mm wafer by using micro-transfer printing on a wafer scale level, as pictured in Fig.3.a, and is also compatible with 300-mm technology. The 3-sigma alignment accuracy is 1 μm , but can be improved to 500 nm by using better alignment markers. The printing cycle duration including all the steps, i.e. the device detection, the picking operation, the alignment with the passive architecture, the printing and the stamp cleaning, is 1 min, and can be fully automated.

An example of a fully populated chip from the 200-mm wafer (46 SiN/LN photonic structures), is depicted in Fig.3.b, with a close-up view of a device in Fig.3.c. In the demonstration, eight

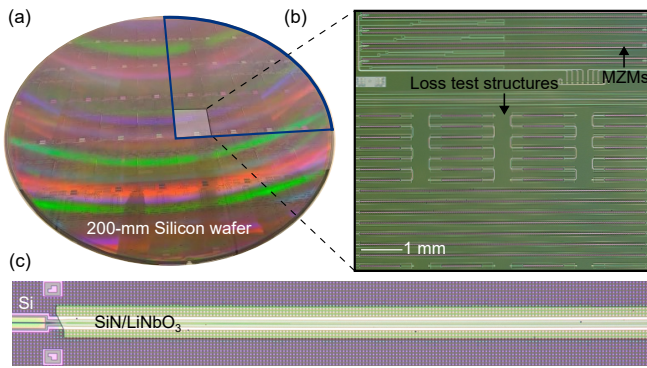


Fig. 3. Demonstration of printing on 200-mm wafers. (a) Photograph of the silicon photonic wafer. (b) Microscope picture of a fully populated die. (c) Zoom on a heterogeneous SiN/LN section.

chips across the wafer were populated. Each die contains cut-back structures to estimate propagation and transition losses, as well as MZMs to verify electro-optic behaviour.

B. Passive characterisation of the hybrid LN/SiN structures

The propagation loss in the hybrid structures is measured using cut-back structures with a 4.2 cm length difference, while the transition loss is determined by comparing the transmission through one device (two transitions) versus the transmission through seven devices (fourteen transitions).

The cut-back structures consist of seven devices each, linked in series, where one has a total length of 4.2 mm (7×0.6 mm) while the other measures 46.2 mm (7×6.6 mm). As the amount of transitions is the same for both, the propagation losses can be extracted by comparing their transmitted power. Using this number, the transition loss can then be extracted by comparing the seven-device series to a single-device structure. The resulting losses, calculated per structure pair are presented in Fig.4, where the propagation loss (Fig.4.a) never exceeds 1 dB/cm, with an average of 0.5 ± 0.1 dB/cm, and a transition loss (Fig.4.b) that measures 0.25 ± 0.01 dB. Both parameters define the hybrid SiN/LN insertion loss to add to the standard passive PDK insertion loss.

In another experiment, unbalanced MZM structures are characterised. Fig.5 shows the transmission spectra of 32 unbalanced heterogeneous Si-SiN/LN MZM modulators (or 64 MZM arms). The insertion loss of the device, stemming from the external and internal silicon routing, the MMI splitters, the transition from Si to SiN/LN and the propagation loss is removed and quantified in the table 1. Heaters were added to the modulator design for tuning, resulting in long internal Si routing. However, these heaters were not used in the scope of this paper as tuning was done by changing the input signal wavelength. The plot is normalised to the maximum grating coupler transmission. A shift in the peak wavelength is observed, coming from the angle variation of the optical fibre over the devices over the wafer due to automatic alignment routines. These results show reproducible results for the modulators.

C. Parallel integration of LN using transfer printing

Another intrinsic aspect of the transfer printing technology is the possibility of the parallel integration of multiple devices. While

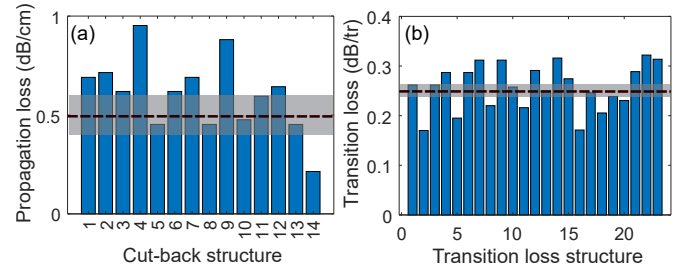


Fig. 4. (a) Measurement of the propagation loss in the SiN/LNO hybrid waveguide. Each data point is based on the comparison between 7×7 mm and 7×1 mm photonic structures. (b) Measurements of the transition loss (from the Si waveguide to the SiN/LN hybrid structures). Each data point is extracted from a measurement of a set of photonic structures (for 7×7 mm and 7×1 mm).

the results presented in the previous section were achieved using a single post for the printing, a mechanical printing test of a 4×7 array of LN photonic structures is realised as an early-stage demonstrator. A dedicated stamp and source are fabricated to match the pitch on the target. The result after the printing operation is depicted in Fig.6. The devices used in this experiment are not characterised since the transferred structures are not optically viable (by design). Nevertheless, the experiment demonstrates the feasibility of the parallel integration of 28 devices within one printing cycle of 1 min and with a misalignment of <1 μ m. This demonstration paves the way for reducing the time for populating a full wafer by orders of magnitude. For example, a typical wafer of 200-mm consisting of 30 dies, where each die can be fully populated in one printing cycle, would take half an hour to fabricate.

4. DISCUSSION AND CONCLUSIONS

The results presented in this paper demonstrate the competitive characteristics of the devices and the scalable nature of LN integration on silicon photonics platforms using transfer printing, in addition to the existing portfolio of monolithic TFLN and TFLN-on-insulator from wafer-bonding technologies. Furthermore, future engineering and R&D efforts are mandatory to exploit the potential of this technique in mature and complex systems, for example, using co-integration with other active devices such as III-V integrated lasers [21, 22], germanium photodetectors [23], UTC-photodiodes [24] or multiplexed structures [25]. The versatility of the approach also allows for direct transfer to emergent thin-film materials such as lithium tantalate [26]. Moreover, emerging progress in this technological field is currently opening the way for cost- and energy-efficient solutions in preparation of the growing demand for data-transmission quantities.

In conclusion, we have demonstrated the fabrication of a heterogeneous Si-SiN/LN unbalanced MZM using micro-transfer printing with competitive characteristics such as an average propagation and transition loss of respectively 0.5 dB/cm and 0.26 dB/transition, ERs of more than 20 dB, a $V_{\pi}L$ of 2.6 V.cm and a bandwidth exceeding 70 GHz for 7 mm LN. Furthermore, we have demonstrated for the first time the integration of LN on a 200-mm wafer, with a printing yield of 99% for over 200 photonic structures, based on the presented approach. A proof-of-concept of parallel integration of 28 devices printed simultane-

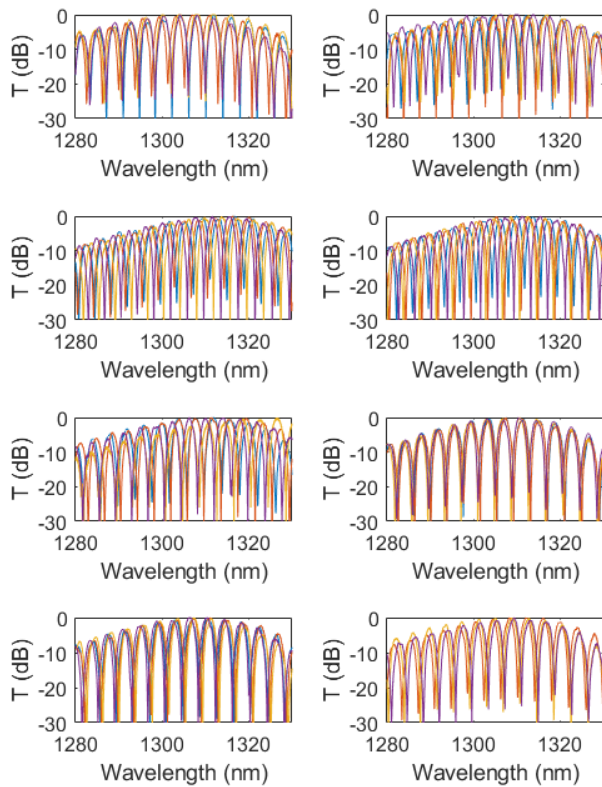


Fig. 5. Example of transmission spectra of 32 heterogeneous Si-SiN/LN interferometers (64 heterogeneous SiN/LN arms) spread over 8 chips from the 200-mm wafer.

ously is also presented to support the efficiency of the technique for an R&D environment. Those results open the way for adding electro-optic materials to the PDK of silicon photonics.

Funding. We want to thank the European Space Agency for funding under the E/0365-70 - NAVISP, LEO Project, the Research Foundation Flanders (FWO) for project 3G035722 and the FWO and F.R.S.-FNRS under the Excellence of Science (EOS) program (40007560).

Acknowledgment. The authors would like to acknowledge the contribution of imec's 200 mm pilot line for silicon photonics wafer fabrication, and the process support team of UGent for the help during the lithium niobate device fabrication.

Disclosures. The authors declare no conflicts of interest.

Data availability. Data underlying the results presented in this paper are not publicly available at this time but may be obtained from the authors upon reasonable request.

REFERENCES

1. S. Lange, S. Wolf, J. Lutz, *et al.*, *J. Light. Technol.* **36**, 97 (2018). Conference Name: Journal of Lightwave Technology.
2. B. Baeuerle, W. Heni, C. Hoessbacher, *et al.*, *Opt. Express* **27**, 16823 (2019). Publisher: Optica Publishing Group.
3. J. M. Estarán, H. Mardoyan, F. Jorge, *et al.*, *J. Light. Technol.* **37**, 178 (2019). Conference Name: Journal of Lightwave Technology.
4. M. Y. S. Sowailam, T. M. Hoang, M. Morsy-Osman, *et al.*, *IEEE Photonics Technol. Lett.* **29**, 442 (2017). Conference Name: IEEE Photonics Technology Letters.
5. P. P. Absil, P. D. Heyn, H. Chen, *et al.*, "Imec iSiPP25G silicon photonics: a robust CMOS-based photonics technology platform," in *Silicon Photonics X*, vol. 9367 (SPIE, 2015), pp. 166–171.

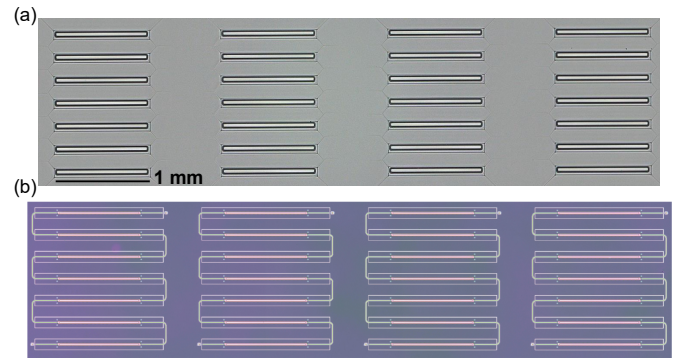


Fig. 6. Demonstration of the parallel integration of LN using transfer printing. (a) Array of 28 stamps. (b) 28 coupons are printed in a printing cycle of 1 min, including picking, aligning, printing and stamp cleaning.

6. D. Chelladurai, M. Kohli, J. Winiger, *et al.*, "Barium Titanate and Lithium Niobate Permittivity and Pockels Coefficients from MHz to Sub-THz Frequencies," (2024). ArXiv:2407.03443 [physics].
7. M. Eppenberger, A. Messner, B. I. Bitachon, *et al.*, *Nat. Photonics* **17**, 360 (2023). Publisher: Nature Publishing Group.
8. C. Haffner, W. Heni, Y. Fedoryshyn, *et al.*, *Nat. Photonics* **9**, 525 (2015). Publisher: Nature Publishing Group.
9. M. Romagnoli, V. Sorianello, M. Midrio, *et al.*, *Nat. Rev. Mater.* **3**, 392 (2018). Publisher: Nature Publishing Group.
10. C. Wu, T. Reep, S. Brems, *et al.*, *IEEE J. Sel. Top. Quantum Electron.* **30**, 1 (2024). Conference Name: IEEE Journal of Selected Topics in Quantum Electronics.
11. K. Powell, X. Li, D. Assumpcao, *et al.*, *Opt. Express* **32**, 44115 (2024). Publisher: Optica Publishing Group.
12. N. Chen, K. Lou, Y. Yu, *et al.*, *Laser & Photonics Rev.* **17**, 2200927 (2023).
13. A. F. Wandesleben, D. Truffier-Boutry, F. Glowacki, *et al.*, *Adv. Eng. Mater.* **26**, 2400396 (2024).
14. M. Churaev, R. N. Wang, A. Riedhauser, *et al.*, *Nat. Commun.* **14**, 3499 (2023). Publisher: Nature Publishing Group.
15. G. Roelkens, J. Zhang, L. Bogaert, *et al.*, *IEEE J. Sel. Top. Quantum Electron.* **29**, 1 (2023). Conference Name: IEEE Journal of Selected Topics in Quantum Electronics.
16. G. Roelkens, J. Zhang, L. Bogaert, *et al.*, *APL Photonics* **9**, 010901 (2024).
17. T. Vandekerckhove, J. D. Witte, L. D. Jaeger, *et al.*, "A scalable quadratic nonlinear silicon photonics platform with printable entangled photon-pair sources," (2025). ArXiv:2503.08783 [physics].
18. T. Vanackere, T. Vandekerckhove, L. Bogaert, *et al.*, *APL Photonics* **8**, 086102 (2023).
19. M. Niels, T. Vanackere, T. Vandekerckhove, *et al.*, *Opt. Mater. Express* **15**, 531 (2025). Publisher: Optica Publishing Group.
20. S. H. Badri, M. V. Kotlyar, R. Das, *et al.*, *Sci. Reports* **15**, 11681 (2025). Publisher: Nature Publishing Group.
21. C. Xiang, W. Jin, O. Terra, *et al.*, *Nature* **620**, 78 (2023). Number: 7972. Publisher: Nature Publishing Group.
22. M. Billet, S. Cuyvers, S. Poelman, *et al.*, *Photonics Res.* **12**, A21 (2024). Publisher: Optica Publishing Group.
23. S. Lischke, A. Peczek, J. S. Morgan, *et al.*, *Nat. Photonics* **15**, 925 (2021). Publisher: Nature Publishing Group.
24. D. Maes, S. Lemey, G. Roelkens, *et al.*, *APL Photonics* **8**, 016104 (2023).
25. G. Gao, D. Chen, S. Tao, *et al.*, *Opt. Express* **25**, 12260 (2017). Publisher: Optica Publishing Group.
26. M. Niels, T. Vanackere, E. Vissers, *et al.*, "A high-speed heterogeneous lithium tantalate silicon photonics platform," (2025). ArXiv:2503.10557 [physics].